



Projected harmful algal bloom frequency in the Yangtze River Estuary and adjacent waters

Haixia Guo, Rongshuo Cai^{*}, Hongjian Tan

Marine Sustainable Development Research Center, Third Institute of Oceanography, Ministry of Natural Resources, Xiamen, 361005, China

ARTICLE INFO

Keywords:

Climate change
Yangtze River Estuary and adjacent waters
Phytoplankton
HAB
BP neural Network
Tipping point

ABSTRACT

Harmful algal blooms (HABs) are a frequent occurrence in China's offshore waters due to climate change and human activity, particularly in the Yangtze River Estuary and adjacent waters. Here, we studied HABs and their relationship with climatic and environmental factors in these waters from 1979 to 2016 using historical observations and reanalysis data. We then projected HABs frequency under various climate scenarios using the "environmental impact factor-frequency of HABs" mathematical model built using the BP neural network method and CIMP5 model data (RCP 2.6, RCP 4.5, and RCP 8.5). The results suggest a significant positive correlation between HABs frequency and seawater nutrient concentration, winter sea surface temperature, and low-wind days, and HABs frequency is anticipated to increase significantly by the 2040s compared with that of the historical era. Furthermore, future phytoplankton conditions are predicted to favor HAB species.

1. Introduction

Harmful algal blooms (HABs) are proliferations of certain noxious and/or toxic microalgae, macroalgae, and cyanobacteria, regardless of their concentration, that cause harm to aquatic ecosystems and human health and wellbeing (GlobalHAB, 2017). The material basis for the occurrence of HABs is an abundance of nutrients in the sea. In addition, specific hydro-meteorological and other seawater physical and chemical factors, such as wind speed and direction, temperature, salinity, dissolved oxygen, and light, influence the occurrence, development, and extinction of HABs (Qi, 2003; Kim et al., 2004; Shen et al., 2010; Zhang et al., 2006).

HAB is one of the major marine ecological hazards in China's near-shore waters. The Yangtze River Estuary (YRE) and adjacent waters experience some of the most frequent HABs in China and are key areas for HAB study. The estuary region, which is the biggest in China, and the nearby seas are dominated by various flow systems and water masses. Among these, the Yangtze River's runoff into the sea forms a sizable freshwater tongue that flushes into the sea, bringing with it abundant nutrients for the growth of HAB species or suspended contaminants that interfere with their photosynthesis. In addition, the sea is affected by the Taiwan warm current and the invasion of the Kuroshio branch of the East China Sea shelf (Cai et al., 2017; Wang et al., 2013). As a result, the convergence zone formed by water systems such as the Yangtze River's

freshwater flush and the warm current originating from Kuroshio jointly influence the HAB prevalence (Zhou et al., 2003). Additionally, the coastal upwelling in the waters along the YRE continuously refills the surface seawater with nutrients, providing a foundation for the development of marine biological resources (Zhu et al., 2003).

HABs in China's nearshore, particularly in the YRE and adjacent waters, have increased significantly at an unprecedented rate since the late 1970s and exhibit significant interdecadal climate change characteristics (Cai et al., 2016). The frequent occurrence of large HABs has seriously impacted the health of the marine environment and ecosystems, as well as their support functions, leading to increased economic losses in coastal areas (Platt et al., 2003; Cai, 2010). According to a previous study, there is an asynchronous shift in the zooplankton biomass and community structure in this sea area, which has created biological conditions that enable spring HABs to more likely occur (Xu, 2004). In addition, the low phosphorus tolerance and strong compensatory growth ability of *Prorocentrum donghaiense*, a bloom-forming planktonic dinoflagellate species, are major causes of HABs in the sea area adjacent to the YRE (Xia et al., 2014). Furthermore, light plays an important role in influencing the growth of dominant HABs algae species under eutrophic conditions (Wang et al., 2008).

In recent years, many studies have used mathematical models to forecast HABs. Since models can quickly approximate high-dimensional nonlinear systems, those built using the backpropagation (BP) neural

^{*} Corresponding author.

E-mail address: cairongshuo@tio.org.cn (R. Cai).

network (error backpropagation learning algorithm) method have become some of the most common methods for predicting HABs (Li et al., 2019; Lou and Huang, 2003; Su et al., 2017; Yang et al., 2003). Although BP models have been demonstrated to be effective in predicting a single HAB, their neural network architecture is typically straightforward, with only one hidden layer and a sparse number of computational nodes. BP neural network models may still be utilized to simulate the frequency of HABs with climate change as long as the neural network structure is tuned for predicting future long-scale HAB frequency instead of a single HAB occurrence. For example, adding hidden layers and computational nodes and screening the training algorithm can improve the model's ability to fit the frequency of long-time HABs. To this end, we first analyzed the attribution of HABs in the YRE and adjacent waters from 1979 to 2016 using historical observations. Next, we used a BP neural network method and determined the optimal structure of the neural network through optimization experiments to construct a mathematical model between the primary influencing factors and the frequency of HABs. Finally, to provide scientific support for HAB ecological disaster risk management in this region, future HABs in the YRE and adjacent waters were predicted using model data from the Coupled International Model Comparison Program 5 (CIMP5) of the Intergovernmental Panel on Climate Change (IPCC).

2. Data and methods

2.1. Overview of the study area and data source

The study area was the YRE and adjacent waters (28°–32°N, 120°–124°E, see Fig. 1). Data on meteorology, climate, marine environment, and other index factors of this sea area were mainly collected

and integrated from a large number of historical data and literature reports, including various field survey observations and satellite remote sensing and reanalysis data, as shown below. The Yangtze River Datong Station's nutrient observations were used to describe the nutrient levels in the study region. This is because the navigation survey concerns temporal discontinuity and spatial variability, which make it challenging to fully satisfy the requirements of mathematical model computation. Additionally, the Yangtze estuary waters' nutrient concentrations are closely related to and show the same variation as those in the Yangtze River freshwater (Wang, 2002; Xin, 2014).

(The sea area within the dashed box is the study area, the blue dot is the Yangtze River Datong hydrological station, and the yellow dots indicate the locations of ground-based meteorological stations)

2.1.1. The HABs

The China Red Tide Disaster Survey and Evaluation (Liang, 2012), as well as the China Marine Disaster Bulletin (<https://www.nmdis.org.cn/hygb/zghyzhgb/>) and the Zhejiang Provincial Marine Disaster Bulletin (<https://www.zjocan.org.cn/oceanswindow/bulletin>) from 2003 to 2016, were the main sources of HAB data used in this study. This includes data on the time of occurrence and location.

2.1.2. Nutrients

The following three nutrient data were gathered at this station:

- Data representing the sum of NO_2^- , NO_3^- , and NH_4^+ is that of dissolved inorganic nitrate (DIN). In this study, we used the historical observation data of DIN from 1962 to 2016 collected at the Datong station in the YRE. Data from 1962 to 1998 and 2002–2008 were obtained from Dai et al. (2011), 2009–2011

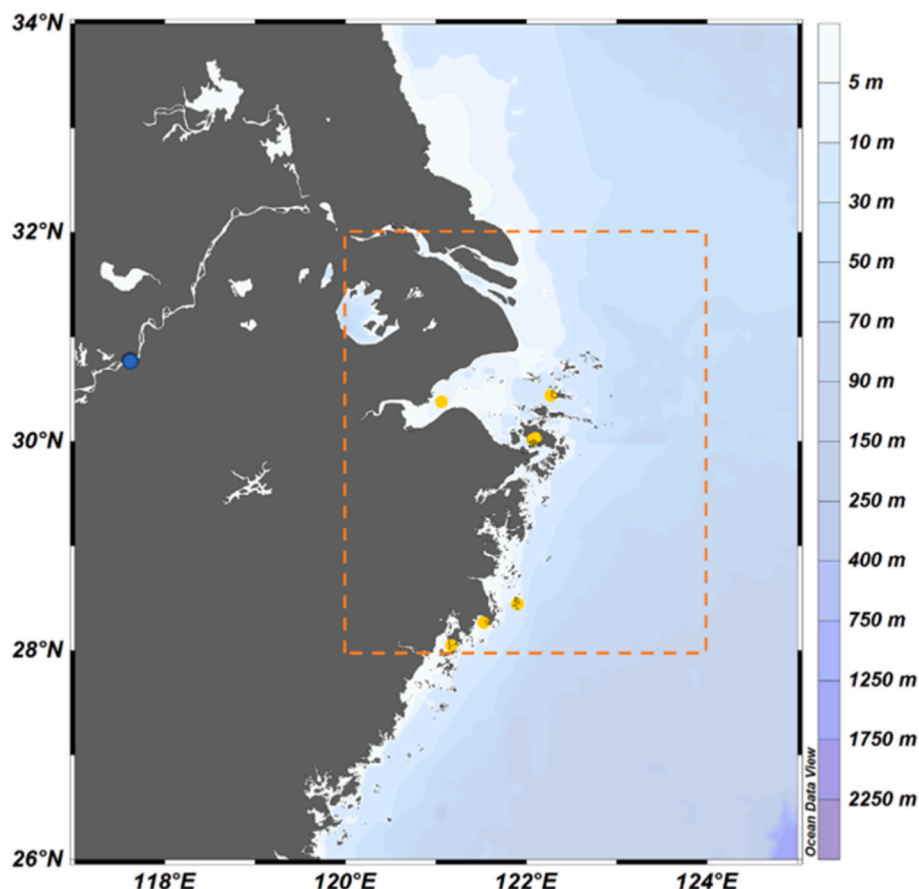


Fig. 1. Yangtze River Estuary and adjacent waters.

from Ding et al. (2019), 1999–2001 and 2012–2013 from Wang et al. (2015), and 2014 and 2016 from Wang et al. (2021).

(b) Dissolved inorganic phosphorus (DIP). Data used in this study were historical DIP observations from 1964 to 2016 at the Datong station, with data for the years 1964–1990, 1998, 2001–2008 obtained from Dai et al. (2011), 2009–2011 from Ding et al. (2019), 1995–1997, 1999–2000, and 2012–2013 from Wang et al. (2015), and 2014–2016 from Wang et al. (2021).

(c) Dissolved silicate (DSi). In this study, we used historical DSi observation data from the Datong station from 1962 to 2016. The data for 1962–1985, 1987, 1998, 2004, 2006, and 2008 were obtained from Dai et al. (2011), 1997–1998 and 2009–2011 from Ding et al. (2019), 1986–2012 from Liang and Xian (2018), and 2014–2016 from Wang et al. (2021).

2.1.3. Wind

The “Daily Surface Climate Information in China Dataset (V3.0)” (<https://data.cma.cn/data/cdcdetail/dataCode/A.0012.0001.html>) released by the National Meteorological Information Center contains wind field data for the sea surface of the YRE and adjacent waters for 1960–2016.

2.1.4. Sea surface temperature (SST)

The Simple Ocean Data Assimilation (SODA) ocean reanalysis datasets, SODA 2.1.6 (http://apdrc.soest.hawaii.edu/datadoc/soda_2.1.6.php), from the University of Maryland, USA, with a time range of January 1958 to December 2008, and SODA 3.4.2 (https://www2.atmos.umd.edu/~ocean/index_files/soda3_readme.htm) with a time range of January 1980 to December 2017 were used in this study.

2.1.5. Photosynthetically available radiation (PAR)

The PAR data used in this study were obtained from the “Chinese photosynthetically available radiation reconstruction dataset 1961–2014 (V1)” published in the Science Data Bank by Liu et al. (2017), which calculates historical solar radiation based on historical observations from Chinese meteorological stations to evaluate and calculate PAR for the period from January 1, 1961, to December 31, 2014 (<https://www.scidb.cn/en/detail?datasetId=633694460953231360>).

2.1.6. Model data

Data on the marine environment under multiple climate scenarios used in this study were derived from the simulation results of the Earth system models in IPCC CMIP5 for historical scenarios and three different greenhouse gas (GHG) emission concentration pathway scenarios (RCP2.6, RCP4.5, and RCP8.5), including SST, wind speed, nutrients, and PAR. Table 1 (available at: <https://esgf-node.llnl.gov/search/cmip5/>) lists the 28 Earth system models from which SST was selected. Because each IPCC CMIP5 model’s given variables, scenarios, time periods, and resolutions are distinct, to thoroughly assess data accessibility, future sea surface wind speed was calculated using MPI-ESM-LR model data for three different GHG emission concentration pathway scenarios (RCP 2.6, RCP 4.5, and RCP 8.5), NO₃ and PO₄ concentrations were calculated using MPI-ESM-LR model data for the current GHG emission concentration pathway scenario (RCP 4.5), and PAR data from the GEOSCCM model for RCP 4.5 were utilized.

2.2. Method

This study used the BP neural network algorithm (Rumelhart, 1986), a multilayer feed-forward network trained according to the error backpropagation algorithm that Rumelhart proposed in 1985. Its primary characteristic is that the mistake propagates backward while the signal is carried forward. There is no feed-forward loop between layers in a BP neural network, and nodes within the same layer are not connected. The weights of each node on the transmission route are modified

Table 1

Information on the 28 CMIP5 global climate models.

Model	Country (Institution)	Resolution (Longitudinal × Latitudinal)	Scenario
ACCESS1-3	Australia (CSIRO)	192 × 145	RCP 4.5, 8.5
CanESM2	Canada (CCCMA)	128 × 64	RCP 2.6, 4.5, 8.5
CMCC-CMS	Italy (CMCC)	192 × 96	RCP 4.5, 8.5
CMCC-CESM	Italy (CMCC)	192 × 96	RCP 4.5, 8.5
CMCC-CM	Italy (CMCC)	480 × 240	RCP 4.5, 8.5
CNRM-CM5	France (CERFACS)	256 × 128	RCP 2.6, 4.5, 8.5
CSIRO-Mk3-6-0	Australia (CSIRO-QCCCE)	192 × 96	RCP 2.6, 4.5, 8.5
CSIRO-Mk3L-1-2	Australia (CSIRO-QCCCE)	192 × 96	RCP 4.5
EC-EARTH	Euro EC-EARTH	320 × 160	RCP 2.6, 4.5, 8.5
FGOALS-s2	China (IAP)	360 × 196	RCP 2.6, 4.5, 8.5
GFDL-CM3	USA (NOAA_GFDL)	144 × 90	RCP 2.6, 4.5, 8.5
GFDL-ESM2G	USA (NOAA_GFDL)	144 × 90	RCP 2.6, 4.5, 8.5
GFDL-ESM2M	USA (NOAA_GFDL)	144 × 90	RCP 2.6, 4.5, 8.5
GISS-E2-H	USA (NASA)	144 × 90	RCP 2.6, 4.5, 8.5
GISS-E2-R-CC	USA (NASA)	144 × 90	RCP 4.5, 8.5
HadGEM2-AO	Korea (NIMR)	192 × 145	RCP 2.6, 4.5, 8.5
HadGEM2-CC	UK (Hadley Centre)	192 × 145	RCP 4.5, 8.5
HadGEM2-ES	UK (Hadley Centre)	192 × 145	RCP 2.6, 4.5, 8.5
INM-CM4	Russia (INM)	180 × 120	RCP 4.5, 8.5
IPSL-CM5A-LR	France (IPSL)	182 × 149	RCP 2.6, 4.5, 8.5
IPSL-CM5A-MR	France (IPSL)	182 × 149	RCP 2.6, 4.5, 8.5
IPSL-CM5B-LR	France (IPSL)	182 × 149	RCP 4.5, 8.5
MIROC-ESM	Japan (MIROC)	128 × 64	RCP 2.6, 4.5, 8.5
MPI-ESM-LR	German (MPI)	192 × 96	RCP 4.5, 8.5
MPI-ESM-MR	German (MPI)	192 × 96	RCP 2.6, 4.5, 8.5
MRI-CGCM3	Japan (MRI)	320 × 160	RCP 2.6, 4.5, 8.5
MRI-ESM1	Japan (MRI)	128 × 64	RCP 8.5
NorESM1-ME	Norway (NCC)	144 × 96	RCP 2.6, 4.5, 8.5

in accordance with the error if the difference between the output and expected result is greater than the predetermined value.

The capacity to obtain highly accurate global approximations to characterize complex, nonlinear, and uncertain systems distinguishes BP neural network algorithms from other nonlinear approaches (Cheng et al., 2015). A four-layer BP neural network was used in this study to simulate HABs in the YRE and adjacent waters under various historical and future climatic scenarios and to manage the intricate link between the primary factors impacting HABs and their frequency.

3. Results and discussion

3.1. Attribution analysis of HABs

The mechanisms of HAB occurrence are still poorly understood. HAB is widely thought to be caused by seawater eutrophication, with changes in hydro-meteorological and physicochemical variables serving as significant contributing causes (Qi, 2003). Our results indicated that the YRE and adjacent waters have SSTs that are often higher than 18 °C at the start of HAB. Frequently, the water temperature rises during the onset of a HAB, and this rapid rise in temperature over a brief period may encourage the growth of harmful algal cells. The salinity of water at the start of a HAB is generally between 23 and 30, and commonly decreases. The wind is often weak during the beginning of HABs, which allows the algae cells to remain in place and congregate (Ye et al., 2009; Zhang et al., 2016). HABs are directly correlated with light, and the cumulative average time of 5–6 days of light is often above 30 h for huge

and extremely large HABs in the sea around the Yangtze River mouth (Ye et al., 2009). The East China Sea HABs correlate strongly with the interdecadal fluctuation of winter winds and SSTs in East Asia. In particular, the pre-winter change in marine atmospheric conditions off China may have a significant impact on the HABs in the spring and summer that follow (Cai et al., 2017, 2022; Cai and Fu, 2018).

Based on the findings of the aforementioned analysis and literature review, we compiled 208 HABs with specific dates of occurrence reported in the YRE and adjacent waters, extracted the average near-surface wind speed during the occurrence of HABs, and performed a box plot analysis (Fig. 2). We then used the upper quartile of 3.646 m/s as the threshold wind speed value (McGill et al., 1978) and counted the days in the months with high occupancy where the daily average wind speed was less than this threshold value, the so-called “low-wind days” (LWD). The YRE and adjacent waters’ winter (December, January, and February, DJF) SST was identified as the temperature indicator influencing HABs (Cai et al., 2017, 2022; Cai and Fu, 2018). Additionally, the PAR of the YRE and nearby waters in months with high HAB occurrence was used as the light indicator affecting HABs, and the nutrient concentration at the Datong station of the YRE was used as the nutrient indicator affecting HABs. Fig. 3 correlates the five environmental indicators to the number of HABs observed in recent years.

As shown in Fig. 3, the YRE’s nutrient concentrations have generally increased significantly since 1962 due to the estuary’s growing eutrophication as a result of human activities. Over the past 50 years, the DIN and DIP concentrations have increased by approximately 154.64 and 1.84 $\mu\text{mol/L}$, respectively, while changes in the DSI concentration are less obvious. The frequency of HABs in the YRE and adjacent waters increased dramatically at an unprecedented rate between 1979 and 2020, reaching two peak values in 1990 (32 times) and 2003 (86 times), showing interdecadal growth and a notable decreasing trend after 2003. This increase in frequency is also shown in Fig. 3. The YRE and adjacent waters had a large interdecadal downward shift in near-surface wind speed from 1970 to 2014 but an interdecadal rise in the frequency of LWD (Cai et al., 2017). A considerable interdecadal increase in winter SST was also seen in the

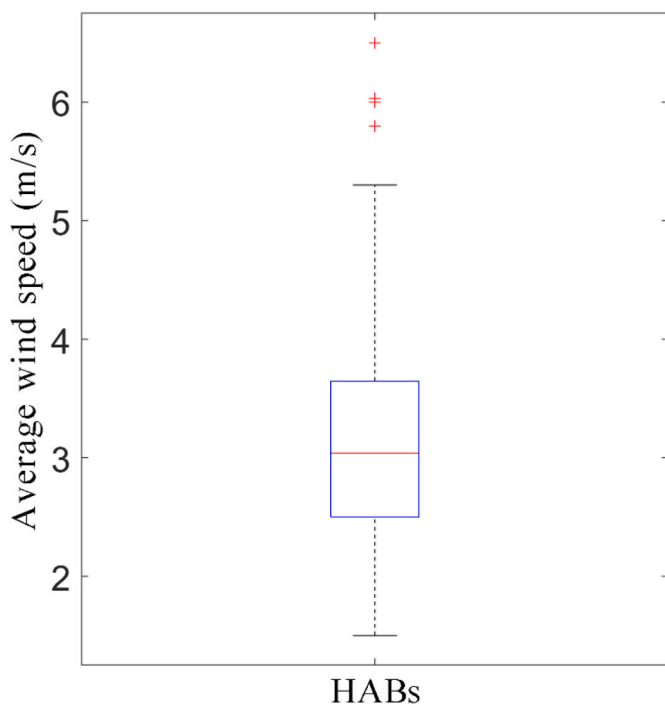


Fig. 2. Average wind speed during HABs.

YRE and adjacent waters beginning in 1970, and this pattern changed to a declining one after 2004, changing along with the frequency of HABs, although there was no discernible trend in PAR. The correlation study (Table 2) revealed a modestly positive link between HABs and PAR during the past 40 years but a strong positive correlation with environmental impact parameters, including pre-winter SST, pre-winter nutrient concentration, and LWD frequency.

Due to the development of human activities since the 1980s, the eutrophication of seawater in the YRE and adjacent waters has dramatically increased, and the phytoplankton density has displayed a significant interannual fluctuation (Yang and Xu, 2015). According to the aforementioned studies, under such eutrophic environments, wind speed and SST may be significant variables limiting the occurrence of HABs in the YRE and adjacent waters. Furthermore, related research indicates that the East Asian monsoon weakens interdecadally, which impacts the capacity of surface seawater offshore China to mix. Moreover, the East China Sea HABs closely match the interdecadal variation in East Asian winter winds and SSTs (Cai et al., 2017; Cai and Fu, 2018). The weakening of the low-level wind field of the East Asian monsoon makes the sea surface wind correspondingly weaker, thus creating an environment conducive to the accumulation and burgeoning proliferation of HABs organisms.

3.2. Mathematical model construction, simulation, and validation of the frequency of HABs

The simulation experiments in this research were mostly conducted using the Matlab 2020b BP neural network function, and the mathematical model was based on a four-layer neural network with double hidden layers. Five environmental factor variables, including DIN, DIP, SST (DJF), LWD, and PAR, were chosen as input layers based on the findings of the attribution analysis in Section 3.1,¹ and the model was trained using historical environmental factor variables-HAB frequency data. According to Fig. 4, using the data from future environmental factors, the built-in model was then used to simulate changes in the frequency of future HABs.

A total of 5×38 node values of environmental factor variables from 1979 to 2016 were used to evaluate the simulation results of the constructed model (individual missing measurement points were filled by linear interpolation with adjacent nodes). Twelve years of data (about 30%) were randomly chosen as the test set to assess the model, and the other 26 years of data (about 70%) were used as the training set for the model training. The simulation data in Table 3 demonstrates that there is a minimal absolute difference between the anticipated value and the model output value, with a mean absolute error (MAE) of approximately 5.87, a root mean square error (RMSE) of 7.53, and a coefficient of determination (R^2) of 0.71. Therefore, the simulated value seems more practical in recreating the historical variable characteristics of the frequency of HABs in the YRE and adjacent waters (Fig. 5). Furthermore, as shown in Fig. 6, the validation outcomes demonstrate that the model output values closely match the anticipated values. Thus the neural network model developed in this study can accurately replicate the historical fluctuation of HABs frequency in the YRE and adjacent waters using environmental element variables (DIN, DIP, SST [DJF], LWD, and PAR).

3.3. Simulation results and analysis of the frequency of future HABs

The future environmental factor variables (DIN, DIP, SST [DJF], LWD, and PAR) under different climate scenarios (RCP 2.6, RCP 4.5, and RCP 8.5) were input into the constructed neural network model to simulate the changes in the frequency of HABs in the YRE and adjacent

¹ DSI was not taken into account in this experiment since the DSI environment variable is absent from the CMIP5 future model data.

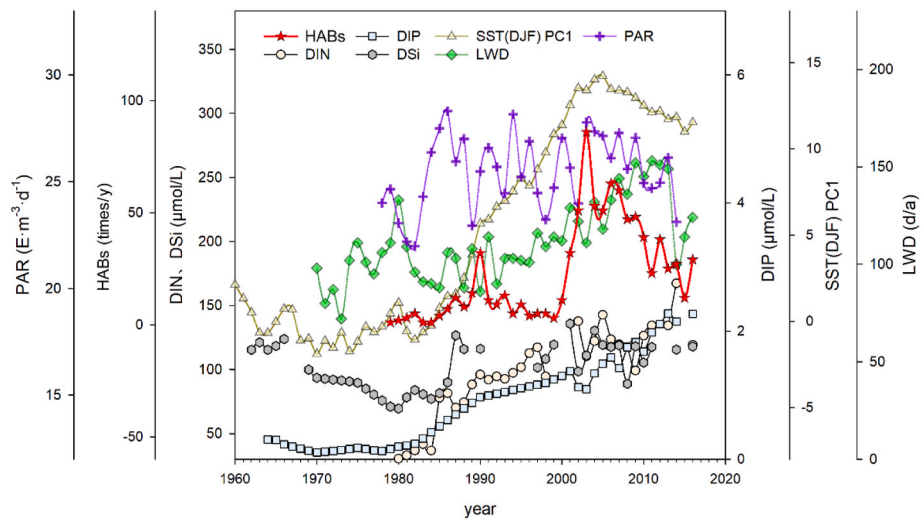


Fig. 3. Relationship between the number of HABs and environmental impact factors in the Yangtze River Estuary and adjacent waters
 Note: PC1 is the first time series of the empirical orthogonal function.

Table 2
 Correlations between the number of HABs and environmental impact factors in the Yangtze River Estuary and adjacent waters.

Factors	DIN	DIP	DSi	SST (DJF) PC1	LWD	PAR
Correlation coefficient	0.609	0.536	0.523	0.729	0.535	0.310
P	< 0.001	< 0.001	< 0.001	< 0.001	< 0.001	0.066

waters under different greenhouse gas emission concentration scenarios in this century. However, there is a lack of future PAR data under the RCP 2.6 and 8.5 scenarios, as well as future seawater nutrient data under the RCP 2.6 scenario, among the data from the CIMP5 model. Given that PAR is less sensitive to temperature changes and stratification caused by temperature increases in low-latitude shallow shelf waters, which have a much smaller impact on seawater nutrients than in deep waters (Dutkiewicz et al., 2013), we used future seawater nutrient and PAR data

under the RCP 4.5 scenario, focusing on the effects of different climate scenarios, especially SST and wind field, on the frequency of future HABs in the YRE and adjacent waters. The simulation results are shown in Fig. 7.

According to the modeling results in Fig. 7, there are three main stages of change in the frequency of future HABs in the YRE and adjacent waters. For example, under the RCP 4.5 scenario in the 2020s, the frequency of HABs oscillated at a low level, averaging approximately 18 ± 12 times/y. However, from the 2030s onwards, the frequency of HABs entered a phase of rapid increase, especially in the 2040s when the frequency of HABs increased to approximately 111 ± 22 times/y, with a quantitative change that seemed to reach a peak. In approximately 25 years, the frequency of HABs increased more than 93 times/y, and after the 2040s, it generally remained at more than 100 times/y; in the 2080s and after, it increased to 140 ± 27 times/y, which was approximately 54 times/y higher than the historical extreme (86 times/y). In contrast, the RCP 2.6 scenario showed a decline in the frequency of HABs, with an average decrease of approximately 10 times/y in 2020–2040 and 21

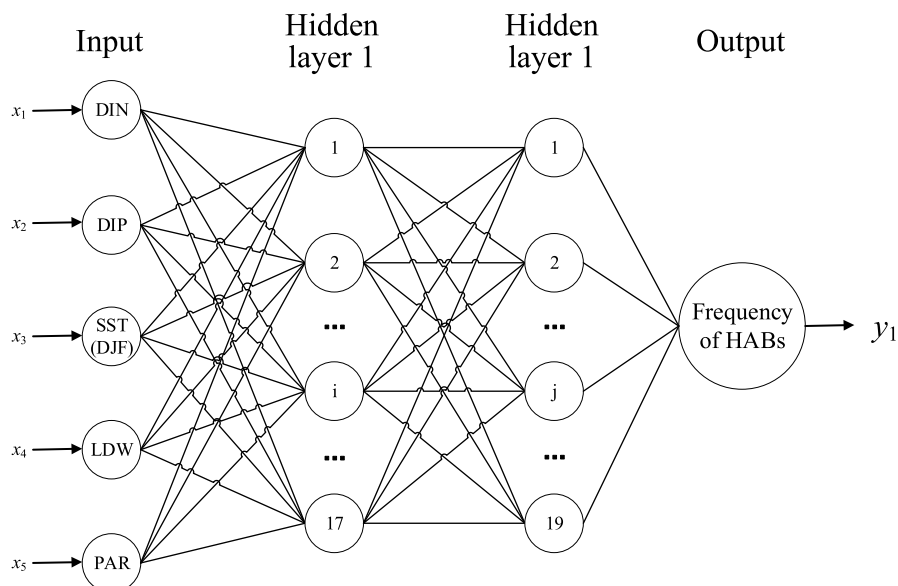


Fig. 4. Scheme of BP neural network structure.

Table 3
Model test results.

Year	Frequency of HABs	Modeled values	Absolute error
1981	3	3.33	0.33
1986	7	3.02	3.98
1987	12	13.96	1.96
1988	8	16.23	8.23
1994	5	2.43	2.57
1995	9	2.74	6.26
1997	5	5.78	0.78
1999	3	3.05	0.05
2002	51	41.90	9.10
2005	51	36.56	14.44
2010	39	24.13	14.87
2013	25	19.13	5.87

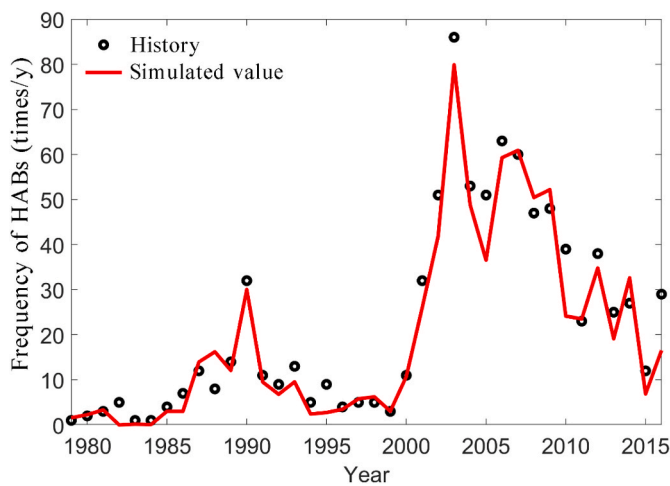


Fig. 5. Historical (1979–2016) HAB frequency simulated by BP neural network.

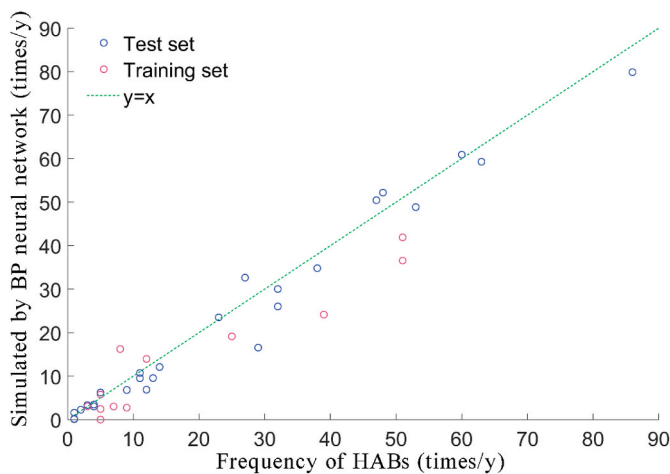


Fig. 6. BP neural network simulation verification.

times/y in 2040–2089. The frequency of HABs rose under the RCP 8.5 scenario compared with that under RCP 4.5, with a modest increase in frequency in 2020–2040 but an average increase of approximately 13 times/y in 2040–2089. In general, HABs in the YRE and adjacent waters are predicted to increase rapidly in the 2030s and leapfrog after the 2040s; in addition, the frequency of HABs rises with an increase in greenhouse gas emission concentration, i.e., according to RCP 2.6, RCP 4.5, and RCP 8.5 scenarios.

3.4. The causes of future HABs in the Yangtze River Estuary and adjacent waters

The time series of the input and output layer data are further presented in Fig. 8 to more clearly discuss and visually compare the relationship between the frequency of future HABs and environmental impact factors in the YRE and adjacent waters. Fig. 8b and c shows the future trends of SST and LWD in the YRE and adjacent seas under different climate scenarios. Among them, the SST shows a significant upward trend in winter from the 2020s to the end of this century and reaches 2.26 ± 0.15 , 2.70 ± 0.09 , and 2.94 ± 0.1 °C in the 2040s (corresponding to RCP 2.6, 4.5 and 8.5 scenarios, respectively, relative to the historical period 1986–2005). Thereafter, there is an acceleration in the trend of rising SST, which is considerable in the RCP 4.5 and 8.5 scenarios and is comparable to increases in the frequency of HABs. In addition, LWD during the peak HABs season basically remained in the range of 120–130 days. Fig. 8d and e shows the long-term changes in nutrient salts in the future of the YRE and adjacent waters under the RCP 4.5 scenario. Among these changes, the DIN concentration increased from an average of approximately 124.16 ± 16.37 μmol/L in the 2020s to approximately 133.15 ± 17.45 μmol/L in the 2040s and then decreased to approximately 118.59 ± 17.26 μmol/L in the 2080s. In addition, the DIP concentration increased from an average of approximately 1.773 ± 0.141 μmol/L, increasing to approximately 1.983 ± 0.235 μmol/L in the 2040s, and then decreasing to approximately 1.727 ± 0.200 μmol/L in the 2080s. In the next 20 years or more, there may be a strong correlation between the increases in SST and nutrient concentration and the rapid increase in the frequency of HABs in the YRE and adjacent waters. The ratio of N and P changed from 63.24:28.15 in 2020 to 70.43:5.72 in 2089, as shown in Fig. 8f.

It has been hypothesized that the warming of seawater over the course of this century may result in a significant loss of phytoplankton diversity in the (sub)tropics of the northern hemisphere (Thomas et al., 2012). Moreover, some larger phytoplankton species are gradually declining or even facing the threat of extinction owing to changes in the structure of the nutrient supply, while some smaller phytoplankton types are becoming more and more dominant, which may result in the extinction of up to 30% or more diatom types (Henson et al., 2021). Because diatoms and dinoflagellates have different ecological niche characteristics, changes in nutrient structure caused by global warming, such as higher nitrogen to phosphorus ratios, favor the rapid growth of dinoflagellates (Xiao et al., 2019). This suggests that the East China Sea’s phytoplankton community structure will likely become more homogeneous as a result of changes in miniaturization and declining diversity. According to the analysis presented above, under the RCP 2.6, 4.5, and 8.5 scenarios, the phytoplankton ecosystem in the YRE and adjacent waters may change in the 2040s to a more hospitable environment for the survival of HAB species that are adapted to rising SST and changes in nutrient structure. It seems probable that the new “equilibrium” condition of the phytoplankton ecosystem, with regards to HAB prevalence, is preferable. This means that the marine environment in the YRE and adjacent waters is progressively losing its original equilibrium state, and around 2040, it may be the climate threshold year for the planktonic ecology to significantly shift as a result of global warming. There may be several irreversible changes in the marine ecosystem when it reaches its climate tipping point, increasing the danger of ecological and environmental calamities that are now hard to anticipate (Cai et al., 2021).

4. Conclusions

This study explored the relationship between environmental factors and the frequency of HABs in the YRE and adjacent waters from 1979 to 2016. It did so using historical observation and reanalysis data and built a mathematical model of “environmental impact factor - frequency of HABs” using the BP neural network method to simulate and predict the frequency of HABs under different climate scenarios. Our findings were as follows:

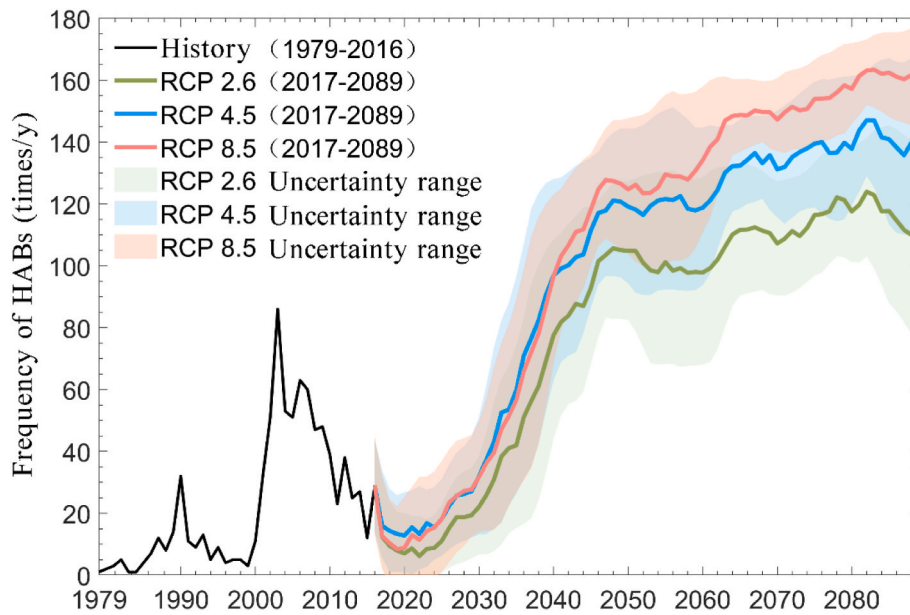


Fig. 7. History and future frequency of HABs in the Yangtze River Estuary and adjacent waters during simulated by BP neural network.

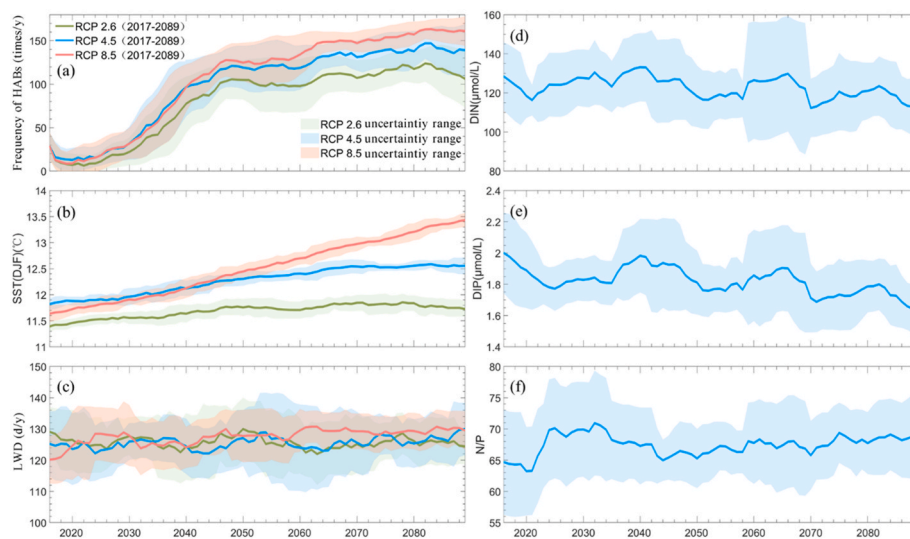


Fig. 8. Time series of the future frequency of HABs in the Yangtze River Estuary and adjacent waters under different climate scenarios (RCP 2.6, RCP 4.5, and RCP 8.5) (a), and the environmental impact factors such as SST (b), days of light wind (c), DIN (d), DIP (e), and N/P (f).

- 1) According to the HABs attribution analysis, there has been a significant positive correlation over the past 40 years between the frequency of HABs and environmental impact factors such as nutrient concentration, SST (DJF), and LWD in the YRE and adjacent waters.
- 2) The mathematical model of “environmental impact factor - frequency of HABs” constructed using the BP neural network algorithm can more accurately capture the historical changes of HABs in the YRE and adjacent waters. In addition, the simulation is relatively accurate since the performance measurements of the RMSE is 7.53, the MAE is 5.87, and $R^2 = 0.71$.
- 3) The simulation prediction results show that under three climate scenarios (RCP2.6, RCP4.5, and RCP8.5), the SST warming reaches 2.26 ± 0.15 , 2.70 ± 0.09 , and 2.94 ± 0.16 °C, respectively, by approximately 2040, relative to the historical period, and continues to rise thereafter. Meanwhile, the frequency of HABs in the YRE and adjacent waters increased significantly, reaching 92 ± 7 , 111 ± 22 ,

and 118 ± 17 times/y for the aforementioned climate scenarios, respectively.

- 4) Under different climate scenarios, the continued warming of the YRE and adjacent waters around 2040 is likely to cause a shift in the phytoplankton ecosystem from one state to another, creating an environment conducive to the growth of HAB species such as dinoflagellates, which can adapt to rising SST and changes in nutrient structure.
- 5) The Yangtze River’s Three Gorges Dam significantly impacted the phytoplankton ecosystem in the estuary and adjacent waters (Ding et al., 2019; He et al., 2022; Jiang et al., 2014), but that impact gradually subsided after almost two decades. It is unknown, however, whether the significant warming of the waters relative to the historical period, such as around 2040, will cause a shift in the state of the phytoplankton ecosystem in the future, including a significant increase in the frequency of HABs.

Author statement

Haixia Guo: Methodology, Software, Data curation, Formal analysis, Writing- Original draft, Investigation, Visualization, Writing- Reviewing and Editing **Rongshuo Cai:** Conceptualization, Supervision, Project administration, Writing- Original draft, Writing- Reviewing and Editing **Hongjian Tan:** Data curation, Validation, Investigation.

Declaration of competing interest

The authors declare that they have no known competing financial interests or personal relationships that could have appeared to influence the work reported in this paper.

Data availability

Data will be made available on request.

Acknowledgments

This work was funded by the National Key Research and Development Program of China (2017YFA0604902). The authors are very grateful to Dr. John E. Hay (University of the South Pacific, Cook Islands Campus, Cook Islands) and Dr. Harilaos Kontoyiannis (Hellenic Center for Marine Research, Greece) for their helpful comments and edits regarding an earlier draft of this paper.

References

- Cai, R., Tan, H., Kontoyiannis, H., 2017. Robust surface warming in offshore China Seas and its relationship to the East Asian monsoon wind field and ocean forcing on interdecadal time scales. *J. Clim.* 30, 8987–9005.
- Cai, R., Tan, H., Qi, Q., 2016. Impacts of and adaptation to inter-decadal marine climate change in coastal China seas. *Int. J. Climatol.* 36, 3770–3780.
- Cai, R., 2010. *The Influence of Climate Change on Chinese Offshore Ecology System*. Ocean Press, Beijing.
- Cai, R., Fu, D., 2018. The pace of climate change and its impacts on phenology in Eastern China. *Chin. J. Atmos. Sci.* 42, 729–740.
- Cai, R., Tan, H., Guo, H., 2022. *Climate Change and Primary Production Offshore China - Impacts, Adaptation and Vulnerability*. Science Press, Beijing.
- Cai, R., Wang, H., Zheng, H., Guo, H., Amro, A.E., 2021. Action against climate tipping points: carbon neutrality. *China Popul. Resour. Environ.* 31, 16–23.
- Cheng, C., Cheng, X., Dai, N., Jiang, X., Sun, Y., Li, W., 2015. Prediction of facial deformation after complete denture prosthesis using BP neural network. *Comput. Biol. Med.* 66, 103–112.
- Dai, Z., Du, J., Zhang, X., Su, N., Li, J., 2011. Variation of riverine material loads and environmental consequences on the Changjiang (Yangtze) estuary in recent decades (1955–2008). *Environ. Sci. Technol.* 45, 223–227.
- Ding, S., Chen, P., Liu, S., Zhang, G., Zhang, J., Dan, S.F., 2019. Nutrient dynamics in the changjiang and retention effect in the three Gorges reservoir. *J. Hydrol.* 574, 96–109.
- Dutkiewicz, S., Scott, J.R., Follows, M., 2013. Winners and losers: ecological and biogeochemical changes in a warming ocean. *Global Biogeochem. Cycles* 27, 463–477.
- GlobalHAB, 2017. *Global harmful algal blooms, science and implementation plan*. Del. Paris : SCOR IOC 64.
- He, Y., Wang, Y., Wu, H., 2022. Regulation of algal bloom hotspots under mega estuarine constructions in the Changjiang river estuary. *Front. Mar. Sci.* 8, 791956.
- Henson, S.A., Cael, B.B., Allen, S.R., Dutkiewicz, S., 2021. Future phytoplankton diversity in a changing climate. *Nat. Commun.* 12, 1–8.
- Jiang, Z., Liu, J., Chen, J., Chen, Q., Yan, X., Xuan, J., Zeng, J., 2014. Responses of summer phytoplankton community to drastic environmental changes in the Changjiang (Yangtze River) estuary during the past 50 years. *Water Res.* 54, 1–11.
- Kim, D.-I., Matsuyama, Y., Nagasoe, S., Yamaguchi, M., Yoon, Y.-H., Oshima, Y., Imada, N., Honjo, T., 2004. Effects of temperature, salinity and irradiance on the growth of the harmful red tide dinoflagellate *Cochlodinium polykrikoides* Margalef (Dinophyceae). *J. Plankton Res.* 26, 61–66.
- Li, H., Liu, T., Shao, Z., Huang, H., 2019. Application of a BP neural network based on decision tree and two partition algorithm in prediction of red tide severity. *Mar. Sci.* 43, 34–40.
- Liang, Y., 2012. *Investigation and Evaluation of Red Tide Hazards in China*. Ocean Press, Beijing.
- Liu, H., Tang, L., Hu, B., Liu, R., Wang, Y., 2017. *China Reconstruction of Photosynthetically Active Radiation Data Collection 1961–2014 (V1)*. Science Data Bank.
- Lou, X., Huang, W., 2003. An artificial neural network method for detecting red tides with NOAA AVHRR Imagery. *J. Remote Sens.* 7, 125–130.
- Liang, C., Xian, W., 2018. Changjiang nutrient distribution and transportation and their impacts on the estuary. *Contin. Shelf Res.* 165, 137–145.
- McGill, R., Tukey, J.W., Larsen, W.A., 1978. Variations of box plots. *Am. Statistician* 32, 12–16.
- Platt, T., Fuentes-Yaco, C., Frank, K.T., 2003. Spring algal bloom and larval fish survival. *Nature* 423, 398.
- Qi, Y., 2003. *Red Tide off China's Coast*. Science Press, Beijing.
- Rumelhart, D.E., 1986. Learning representation by BP errors. *Nature* 64–70.
- Shen, L., Xu, H., Wu, P., 2010. Study on marine environmental character of Changjiang Estuary and adjacent East China Sea during algal blooms. *Mar. Environ. Sci.* 29, 631–635.
- Su, X., Jin, F., Yang, Q., Chen, H., Yu, X., Li, X., Guo, M., Liu, Q., Luo, J., 2017. Red tide forecasting model based on BP neural network in Fujian sea area. *J. Fish. China* 41, 1744–1755.
- Thomas, M.K., Kremer, C.T., Klausmeier, C.A., Litchman, E., 2012. A global pattern of thermal adaptation in marine phytoplankton. *Science* 338, 1085–1088.
- Wang, J., Yan, W., Chen, N., Li, X., Liu, L., 2015. Modeled long-term changes of DIN: DIP ratio in the Changjiang River in relation to Chl- α and DO concentrations in adjacent estuary. *Estuar. Coast Shelf Sci.* 166, 153–160.
- Wang, Y., Liu, D., Xiao, W., Zhou, P., Tian, C., Zhang, C., Du, J., Guo, H., Wang, B., 2021. Coastal eutrophication in China: trend, sources, and ecological effects. *Harmful Algae* 107, 102058.
- Wang, A., Wang, X., Han, X., Li, Y., Zhu, C., 2008. Effects of solar radiation on the growth and succession of harmful algae in the East China Sea in spring. *Mar. Environ. Sci.* 27, 144–148.
- Wang, B., 2002. Distributions and transportation of nutrients in Changjiang River Estuary and its adjacent sea areas. *Acta Oceanol. Sin.* 24, 53–58.
- Wang, Q., Chen, J., Jin, H., Li, H., Gao, S., Lu, Y., Xu, J., Weng, H., 2013. Nutrient structure and limitation in changjiang River Estuary and adjacent East China sea. *Acta Oceanol. Sin.* 35, 128–136.
- Xu, Z., 2004. Relationship between red tide occurrence and zooplankton communities structure in the coastal sea of East China Sea in spring. *China Environ. Sci.* 24, 257–260.
- Xia, R., Xu, Z., Gao, Q., 2014. Compensatory growth of *Prorocentrum donghaiense* Lu under nitro-gen and phosphorus deficiency stress. *J. Fish. Sci. China* 21, 1200–1210.
- Xiao, W., Laws, E.A., Xie, Y., Wang, L., Liu, X., Chen, J., Chen, B., Huang, B., 2019. Responses of marine phytoplankton communities to environmental changes: new insights from a niche classification scheme. *Water Res.* 166, 115070.
- Xin, M., 2014. *Long-term Variations of Key Environmental Factors and Their Ecological Effects in the Changjiang Estuary*. Ocean University of China, Qingdao.
- Yang, J., Luo, X., Ding, D., Qin, Q., 2003. A preliminary study on artificial neural network method for predicting red tide. *Adv. Mar. Sci.* 21, 318–324.
- Yang, Y., Xu, R., 2015. The environment variation trend in the Changjiang River Estuary in the past 30a. *Mar. Sci.* 10, 101–107.
- Ye, J., Zhou, L., Chen, S., Ye, J., 2009. Meteorological factors related to the red tide in Zhoushan sea area. *Mar. Forecasts* 26, 76–82.
- Zhang, F., Yao, Y., Ma, L., 2016. Analysis on hydro-meteorological conditions and characteristics of red tide in Wenzhou coastal waters. *Mar. Forecasts* 33, 89–94.
- Zhang, J., Bai, Y., Yu, J., Pang, H., Deng, W., Li, H., Wu, D., Zhao, X., Chen, H., Jiang, Y., 2006. Forecast of red tide in the South China Sea by using the variation trend of hydrological and meteorological factors. *Mar. Forecasts* 8, 60–74.
- Zhou, M., Yan, T., Qu, J., 2003. Preliminary analysis of the characteristics of red tide areas in Changjiang River estuary and its adjacent sea. *Chin. J. Appl. Ecol.* 14, 1031–1038.
- Zhu, G., Xu, W., Zhu, D., Shi, Q., Zhang, J., 2003. Distribution of phytoplankton and water dynamical environmental factors in high red tide occurrence area of Changjiang River estuary. *Chin. J. Appl. Ecol.* 14, 1135–1139.